JOURNAL PRE-PROOF

This is an early version of the article, published prior to copyediting, typesetting, and editorial correction. The manuscript has been accepted for publication and is now available online to ensure early dissemination, author visibility, and citation tracking prior to the formal issue publication.

It has not undergone final language verification, formatting, or technical editing by the journal's editorial team. Content is subject to change in the final Version of Record.

To differentiate this version, it is marked as "PRE-PROOF PUBLICATION" and should be cited with the provided DOI. A visible watermark on each page indicates its preliminary status.

The final version will appear in a regular issue of *Archives of Acoustics*, with final metadata, layout, and pagination.

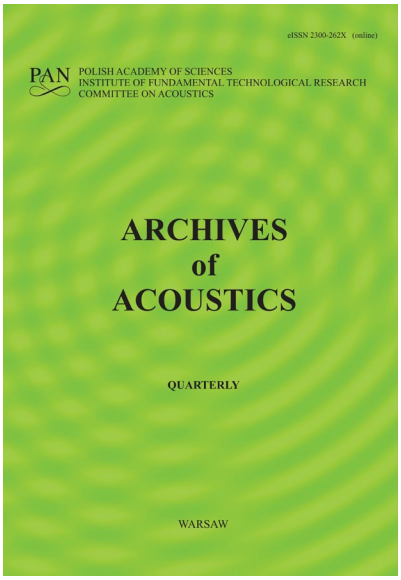

Title: Modeling of High-Speed Ultrasonic Testing of Railway Rails in Track Inspection

Author(s): Sławomir Mackiewicz, Zbigniew Ranachowski, Tomasz Katz, Tomasz Dębowski, Grzegorz Starzyński

DOI: https://doi.org/10.24423/archacoust.2026.4366

Journal: *Archives of Acoustics*

ISSN: 0137-5075, e-ISSN: 2300-262X

Publication status: In press

Received: 2025-10-30

Revised: 2026-02-17

Accepted: 2026-02-26

Published pre-proof: 2026-03-03

Please cite this article as:

Mackiewicz S., Ranachowski Z., Katz T., Dębowski T., Starzyński G. (2026), Modeling of High-speed Ultrasonic Testing of Railway Rails in Track Inspection, *Archives of Acoustics*, https://doi.org/10.24423/archacoust.2026.4366

Modeling of High-Speed Ultrasonic Testing of Railway Rails in Track Inspection

Sławomir MACKIEWICZ[1], Zbigniew RANACHOWSKI[1,*], Tomasz KATZ[1], Tomasz DĘBOWSKI[1], Grzegorz STARZYŃSKI[1]

Sławomir Mackiewicz ORCID: 0000-0003-3826-5365
Zbigniew Ranachowski ORCID: 0000-0003-2447-4705
Tomasz Katz ORCID: 0000-0002-6542-2787
Tomasz Dębowski ORCID: 0000-0002-2394-7331
Grzegorz Starzyński ORCID: 0000-0002-5257-6461

[1]Institute of Fundamental Technological Research Polish Academy of Sciences, Pawińskiego 5B, 02-106 Warsaw, Poland;
*Corresponding Author e-mail: zranach@ippt.pan.pl

Abstract

In the paper the theoretical modeling of ultrasonic testing of railway rails with high scanning speed is considered. The model for the calculation of the ultrasonic field generated by the ultrasonic transducers and the pulse echo amplitude received after wave reflection at the defect is developed. The model is based on well-established principles of elastodynamic theory: the Rayleigh-Sommerfeld integral, the Auld reciprocity relation, and the Kirchhoff approximation. It forms the basis for design of computer program to simulate ultrasonic inspections of railway rails with automated mobile systems. The major innovation introduced in the model is taking into account the high scanning speed of the ultrasonic probes over the rail head and the limited repetition rate of the ultrasonic system. The mentioned aspects of the high-speed rail testing require the revision of one of the basic paradigms of the current ultrasonic models, which assume that the scanning speed of the ultrasonic probe is negligible in comparison to the speed of ultrasonic waves propagating in the tested material. Actually, when scanning rails at a speed of 120 km/h, the ultrasonic probe can change its position up to 5 mm between transmitting and receiving ultrasonic pulses reflected from defects located in the rail foot. Such a shift in probe position is not negligible and should be considered in calculations. As a consequence, the ultrasonic system's slow repetition rate and fast scanning speed can make it less likely that certain rail flaws will be found. To quantitatively examine the severity of these phenomena, the new ultrasonic model and related simulation software was developed.

Keywords: non-destructive testing; railway rails defects; testing of railway rails; automatic ultrasonic testing.

1. Introduction

Due to economic pressure, there is a worldwide trend to increase train speed, traffic density, and axle loads. This has led to an increased rate of defect formation in the railway tracks and rails. The main reason for the increased number of rail defects is rolling contact fatigue (RCF) damages. The most frequent RCF defects occurring in the rail heads are head checking (HC), gauge corner cracking, squats, and transverse head cracking (tache ovale) (Kumar, 2006, UIC Code 712-R, 2002). In order to reduce the risk posed by rail defects, a number of non-destructive testing methods are used. Worldwide implemented rail line testing procedures include such NDT methods as visual, ultrasonic, eddy current, and magnetic (Zumpano and Meo, 2006). In the European Union, the EN Standards (EN 16729-1, 2016, EN 16729-3, 2018) are observed in this respect.

The need of permanent testing of the extensive railway network requires the implementation of fast automated inspection systems and efficient testing procedures. One of the most commonly used techniques is automated ultrasonic inspection capable of scanning the entire rail volume. An example of such an application using the specialized inspection train was described in (Thomas *et al.*, 2007, Heckel *et al.*, 2018). The practical exploitation of the aforementioned equipment revealed that the efficient operation of the system is possible below 80 km/h. Unfortunately, this inspection speed is insufficient for some of the busiest railway lines where trains run at speeds of up to 200 km/h and more. In the dense scheduled train traffic, it is difficult to find a time window for the slow inspection trains. Therefore, the construction of inspection trains capable of performing ultrasonic inspection with speed comparable to express trains is an important and urgent matter. To investigate the possibility of high-speed ultrasonic

inspection of railway rails, extensive research is necessary. The problems involved are not only of purely technical nature, i.e., connected with the construction of more robust scanners and more efficient water coupling systems, but are of more fundamental character. First of all, one should realize that the vast majority of ultrasonic tests performed in today's industry have a quasi-static nature. It means that the scanning speed of the tested object by ultrasonic probes is so slow that we commonly assume that during the transmitting-receiving cycle of the ultrasonic system, the probe is stationary, i.e., is in the same position during the sending and receiving of the ultrasonic pulse. But when we consider ultrasonic scanning of a railway rail with a speed of, say, 120 km/h (33 m/s), the probe position difference between sending and receiving an ultrasonic pulse reflected from the distant defect (located, for example, in the rail foot) can be about 5 mm. It is a value that cannot be neglected, as it is considerably higher than the wavelength produced by typical 2-4 MHz ultrasonic probes used in rail inspections. In other words, the ultrasonic testing model of high-speed inspection must take into account the simultaneous propagation of the ultrasonic pulse in the examination object and the movement of the ultrasonic probe along its surface.

The other important aspect of the high-speed railway rail inspection is the inherent restriction on the system repetition rate (to c.a. 5 kHz) caused by relatively long times of flight of ultrasonic pulses reflected from defects located in the rail neck or foot. Such a restriction of the repetition rate, relatively unimportant for standard ultrasonic testing, causes substantial problems for high-speed inspections of railway rails. Specifically, for ultrasonic testing carried out with a speed of 120 km/h and a system repetition rate of 5 kHz, the scanning step (the distance between successive emissions of ultrasonic pulses along the rail length) is equal to 6.7 mm. If a small defect is located between successive emission points, it can be missed or detected with considerably smaller echo amplitude than would be detected at a standard (slow) scanning

speed. Therefore, a new model of the ultrasonic inspection is needed to take into account the specific problems of ultrasonic testing with high scanning speed.

The paper presents development of ultrasonic pulse-echo testing model which takes into account the dynamic nature of high speed ultrasonic inspection. It can be considered as an extension of our previous quasi static model presented in (Katz, 2021) which was adequate for modelling of ultrasonic tests of railway rails conducted at low scanning speeds.

The model forms the theoretical basis for computer program capable of simulation of high speed ultrasonic inspection of railway rails performed with different types of ultrasonic probes, including shear wave angle beams probes and longitudinal wave normal beam ones. The program allows for calculation of ultrasonic field generated by the probe depending on its parameters (frequency, refraction angle, transducer shape and size, wedge material etc.) as well as calculation of the amplitude of pulse echo reflected from simple model defects (circles or rectangles) of arbitrary size, location and orientation.

In the last part of the paper, some calculation results for typical rail testing configurations are presented and discussed in the context of high scanning speed. Finally, some conclusions, which may be important for designers of high-speed ultrasonic testing systems, are presented.

2. Dynamic model of ultrasonic testing with high scanning speed

As already mentioned, the commonly used model of ultrasonic testing is quasi-static, i.e., it assumes that during the transmitting-receiving cycle, the ultrasonic probe remains in the same position. Thus, any head movement associated with object scanning does not affect the amplitude of the recorded ultrasonic echoes. In such a theoretical approach, the test is carried out in a kind of virtual jump from one wave emission point to another, with the ultrasonic probe effectively frozen at each of these points during the transmission-reception cycle. In case of high scanning speed, it is necessary to move away from this simplified picture and introduce a

dynamic model of ultrasonic inspection that takes into account the simultaneous movement of the ultrasonic pulse and the scanning probe. The scheme of small defect detection in such a model is shown in Fig. 1.

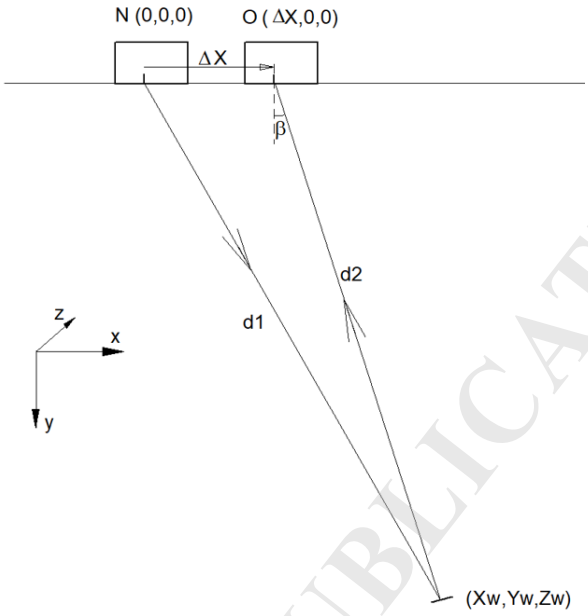

Fig. 1. Defect detection in the dynamic model of ultrasonic testing.

The transmission-reception cycle of the ultrasonic system in the pulse-echo mode can be described as follows. The probe sends an ultrasonic pulse into the tested object in the transmitting position—*N*, which can be described by initial coordinates (0,0,0) in the stationary coordinate system (*X,Y,Z*) associated with the rail. The *X* axis is parallel to the rail axis and is also a scanning axis of the ultrasonic probe; the *Y* axis is directed down the rail, and the *Z* axis is in the transverse direction. The emitted pulse propagates in the rail material at the speed of ultrasonic wave *Vu* and eventually arrives at a material defect located at the point with coordinates (*Xw, Yw, Zw*). The distance **d1** that the ultrasonic pulse travels during this time can be calculated from the geometry of the problem shown in the drawing, remembering, however, that the problem is essentially three-dimensional, i.e., the defect shown does not have to be located in the plane of the drawing:

$$d_1 = \sqrt{{X_w}^2 + {Y_w}^2 + {Z_w}^2}\ . \qquad (1)$$

Consequently, the time t_1 in which the ultrasonic pulse travels from the point of introduction to the defect center can be calculated from the formula:

$$t_1 = d_1/V_u. \qquad (2)$$

While the ultrasonic pulse is propagating to the defect and back, the probe moves along the rail at the scanning speed V_s, covering the distance $\Delta X = V_s(t_1+t_2)$ in that time. However, the distance ΔX cannot be easily calculated because we don't know the time t_2 in which the pulse travels the unknown return distance d_2 from defect to the probe. Regarding Fig. 1, one can see that the two sides of the triangle shown in the figure, ΔX and d_2, are dependent on the unknown time t_2 as follows:

$$\Delta X = V_s(t_1 + t_2) \quad \text{and} \quad d_2 = V_u t_2. \qquad (3)$$

However, all sides of the triangle shown are related by the law of cosines, giving an equation from which the unknown value of t_2 can be calculated:

$${d_1}^2 = \Delta X^2 + {d_2}^2 - 2\Delta X d_2 \cos(90° + \beta). \qquad (4)$$

It should be noted that the angle $(90°+\beta)$ lies in the plane of the triangle, not in the plane of the drawing. Using known trigonometric identities, formula (4) can be transformed into the form:

$${d_1}^2 = \Delta X^2 + {d_2}^2 + 2\Delta X d_2 \sin\beta, \qquad (5)$$

where the unknown value of $\sin\beta$ can be expressed using the formula:

$$\sin\beta = (X_w - \Delta X)/d_2. \quad (6)$$

Substituting this value into formula (5), we get the equation:

$$d_1{}^2 = \Delta X^2 + d_2{}^2 + 2\Delta X X_w - 2\Delta X^2. \quad (7)$$

Then, by substituting the values of ΔX and d_2 expressed by formulas (3), we finally obtain the quadratic equation for the unknown transition time t_2 from the defect to the probe at its receiving position:

$$[V_u^2 - V_s^2]t_2{}^2 + \left[2V_s X_w - \frac{2V_s^2 d_1}{V_u}\right] t_2 + \left[\frac{2V_s d_1 X_w}{V_u} - d_1^2 - \frac{V_s^2 d_1^2}{V_u^2}\right] = 0. \quad (8)$$

By taking the positive root of the above quadratic equation and leaving only the linear terms in the V_s/V_u ratio, we obtain the approximate time of passage t_2

from the defect center to the probe in its receiving position:

$$t_2 = \frac{d_1}{V_u} - 2\frac{V_s}{V_u}\frac{X_w}{V_u}. \quad (9)$$

Knowing times t_1 and t_2, one can easily calculate the probe displacement ΔX during the time of flight of the ultrasonic pulse to and from the considered defect:

$$\Delta X = V_s(t_1 + t_2) = 2V_s\left(\frac{d_1}{V_u} - \frac{V_s}{V_u}\frac{X_w}{V_u}\right), \quad (10)$$

where d_1 is calculated from (1). It should be noted that the displacement ΔX between the points of sending and receiving the ultrasonic pulse depends on both the scanning speed V_s and the location of the defect in the rail in the defined coordination system. The further away the defect is from the probe, the greater the distance between the points of sending and receiving of the reflected ultrasonic pulse.

The presented dynamic model of ultrasonic inspection is not fully strict as it assumes that the ultrasonic probe is effectively frozen during the acts of emitting and receiving ultrasonic pulses. Still, the time of introduction/reception of ultrasonic pulses to the material is very short (c.a. 2 μs for standard 2 MHz ultrasonic probes) as compared to the typical times of flight of ultrasonic pulses reflected from the rail defects (from 20 μs to 150 μs). It means that the model takes into account the major part of the phenomena related to the dynamic nature of the high-speed ultrasonic testing of railway rails. One can also object that the above consideration is not valid for large defects whose size is comparable to the distance between the testing probe and the defect center. Actually, it is not a big problem, as we can divide a large defect into many small fragments and calculate ΔX for each fragment separately. Then the echo amplitude is calculated as the sum of the contributions from all fragments of the larger defect.

The above solution is the basis for the modification of the calculation algorithms implemented in the *SymUT* computer program, prepared by the first author of the paper. The program calculates ΔX values using formula (10) based on the entered data on the scanning speed *Vs* and model defect position relative to the testing probe. Simulations of ultrasonic echo envelopes during rail scanning performed applying the *SymUT* program will be presented in the last section of the paper.

3. Basic assumptions and simplifications adopted in the ultrasonic model

The model assumptions were thoroughly adjusted to the actual conditions of ultrasonic testing of railway rails. Specifically, the tested material was assumed to be a homogeneous, isotropic, elastic solid characterized by ultrasonic velocities, mass density, and attenuation coefficients typical of railway steel. The attenuation coefficient values for longitudinal and transversal waves in rail steel were inferred from the tables given in (Ono, 2020a and 2020b. The probe wedge material was assumed to be a fluid medium with density and longitudinal wave velocity corresponding to actually used solid materials (PMMA or Rexolite). This simplification allowed for the avoidance of unnecessary mathematical complexity in situations where only longitudinal wave propagation in probe wedges is considered.

It was assumed that the boundary between the probe wedge and tested material is perfectly flat, neglecting the slight curvature of the running surface of the rail heads. Additionally, it was assumed perfect acoustic coupling between the probe wedge and tested material (smooth contact boundary conditions sometimes also called slip boundary conditions). They assume continuity of normal stress and displacement and vanishing of tangential stresses at the border. The potential influence of the coupling layer thickness on echo amplitude could be studied separately using the other model described in (Mackiewicz *et al.,* 2024).

Taking into account the considerable size of the tested items (rails), it is assumed that the modeled defects are generally situated in the far fields of ultrasonic probes, i.e., in the region where the ultrasonic field can be locally approximated by the plane wave. On the other hand, the paraxial approximation was avoided as many rail defects are cracks with unfavorable orientation (Deschamps, 1972), which may be better detected by the side rays significantly deviated from the beam axis. In the proposed model, we also assume that the ultrasonic pulses generated by the probe transducers are relatively short, as is actually the case in modern commercial ultrasonic probes. This means that the -6 dB bandwidth of simulated probes should not be smaller than 30%. The first part of the model is a method for the calculation of the

ultrasonic field generated in the tested object by the ultrasonic transducer. Following this basic functionality, the method for calculation of pulse echo amplitude from simple model defects (circle, square, or rectangular cracks) was developed based on the Auld reciprocity principle and Kirchhoff approximation.

4. Calculation of ultrasonic field generated by the ultrasonic transducer

The method of calculation of the ultrasonic field generated by the piezoelectric transducer in the tested material is essentially the same as in the standard quasi-static model. This is because we assumed that the act of introduction of ultrasonic pulse from the probe to the material is short enough that the probe can be considered static during this period of time. After emission, the pulse “forgets” about the sending probe, and it doesn’t matter if the probe is static or travels along the scanning surface with a high speed. So the ultrasonic field generated in the material is independent of this feature and can be calculated in the same way as for stationary probes. Below, the standard geometrical configuration used for ultrasonic testing of railway rails with angle beam shear wave probes will be considered. The calculation for longitudinal wave probes is completely analogue. Because we assumed that the act of introducing of the ultrasonic pulse to the material is very short (compared to the total time of flight in the tested rail) the calculation of the ultrasonic field generated in the material by the moving ultrasonic probe may be performed in the same way as for stationary probe. The probe is coupled to the flat surface of the tested object with a thin layer of coupling medium. The piezoelectric transducer is attached to the refracting wedge made of a formally fluid medium with characteristics (density and longitudinal wave velocity) compatible with plastic material actually used for the fabrication of the refracting wedges (PMMA, polystyrene, or Rexolite). This way the wedge material's shear stiffness can be neglected. This assumption is also compatible with the fact that the probe wedge

is coupled to the tested material with a thin layer of liquid medium which does not transmit shear stresses.

In line with a common practice in ultrasonic modeling, we assume piston-like transducer vibrations with angular frequency ω and uniform particle velocity v_0 over its front surface. The ultrasonic wave propagating in the wedge hits the boundary between the wedge and the tested material at an angle which is the same as the wedge angle α. The wedge angle is selected between the 1st and 2nd critical angles so that only one refracted wave (T-type) is generated in the tested material.

The refraction angle of the transversal wave β is related to the incidence angle of the longitudinal wave α through the Snell's law:

$$\frac{\sin\alpha}{\sin\beta} = \frac{V_{L1}}{V_{T2}} \tag{11}$$

Where V_{L1} is velocity of L-type wave in the wedge material and V_{T2} is velocity of T-type wave in the tested material. (Calmon *et al*., 1998) showed that it is possible to use the Rayleigh-Sommerfeld integral for the calculation of the ultrasonic field in the wedge material. It expresses the acoustic pressure p as an integral over the radiating transducer surface:

$$p(\boldsymbol{x}) = \frac{-i\omega v_0 \rho_1}{2\pi} \int_{S_t} \frac{e^{ikr}}{r}\, dS, \tag{12}$$

where: ρ_1 – mass density of wedge material, ω – angular frequency of ultrasonic vibration, S_t – surface of the transmitting transducer, v_0 – normal particle velocity at the transducer face, k – wavenumber of ultrasonic wave in the wedge and r – distance between the field point and $\boldsymbol{x}$ is current integration point on the transducer surface. Using integral (12), one could easily calculate the ultrasonic field in the wedge material, but not in the tested material. In order to

accomplish this more difficult task, we used the so-called pencil model introduced by (Deschamps, 1972), for calculations of electromagnetic beams generated by radars. This concept was also used for the modelling of ultrasonic waves by (Raillon and Lecoeur-Taibi, 2000) and (Gengembre, 2003). The discussed model has been proved to be very effective in terms of calculation accuracy and computing efficiency. Finally, the ultrasonic field at the point $\boldsymbol{x}$ in the tested material is described by the particle velocity amplitude $\boldsymbol{v}(\boldsymbol{x}, \omega)$ given in the form:

$$v(\boldsymbol{x}, \omega) = \frac{-i\omega v_0}{2\pi V_{L1}} \int_{S_r} \frac{T_{12}^{v}(\alpha) e^{i(k_1 r_1 + k_2 r_2)}}{\left(r_1 + \frac{V_{T2} cos^2\alpha}{V_{L1} cos^2\beta} r_2\right)^{1/2} \left(r_1 + \frac{V_{T2}}{V_{L1}} r_2\right)^{1/2}} dS, \qquad (13)$$

where: V_{L1} – velocity of L-type wave in the wedge material, V_{T2} – velocity of T-type wave in the tested material, α – incidence angle of a pencil central ray at the wedge-material boundary β – refraction angle of a pencil central ray at the wedge-material boundary, r_1 – section of the pencil central ray in the wedge material, r_2 – section of the pencil central ray in the tested material, $k_1 = \omega / V_{L1}$ – wave number of the L- type wave in the wedge material, $k_2 = \omega / V_{T2}$ – wave number of the T- type wave in the tested material, S_r – surface of the radiating transducer and $T_{12}{}^{v}$ is particle velocity transmission coefficient at the wedge-material boundary.

The integral (13) sums up the contributions from partial waves emanating from all vibrating points of the transducer face. The integral sums up the scalar values of particle velocity amplitudes, neglecting the fact that partial waves coming from different points of the transducer surface have particle velocities with slightly different directions. This is a typical simplification

in the scalar theories of diffraction, and its actual meaning in the considered case is illustrated in Fig. 2.

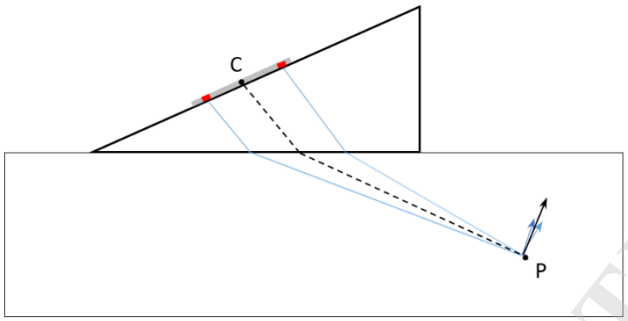

Fig. 2. Polarizations of partial waves coming from different points of vibrating transducer, placed at the top of the wedge.

It can be seen that in the far field, the differences between polarizations of partial waves coming from different parts of vibrating transducers are small, and the simplification made in formula (13) causes only a slight overestimation of the calculated amplitude of the particle velocity of the generated ultrasonic wave. Such scalar values may be conveniently displayed on graphs illustrating the distribution of ultrasonic fields generated by different probes. For more advanced simulations, and specifically for the calculation of ultrasonic echo amplitudes from model defects, we need to know not only wave amplitude but also its polarization. Based on heuristic reasoning, without a rigorous proof, we assume that the polarization of the ultrasonic wave generated by the whole vibrating transducer at a given point P is the same as the polarization of the partial wave emanating from the transducer center and coming to the same point P (see Fig. 2). This assumption, together with formula (13), gives the full description of the ultrasonic field generated in an isotropic solid by an angle beam shear wave probe.

All factors included in integral (13) can be readily calculated if we can determine α, β, r_1 and r_2 for any combination of a source point on the transducer surface and evaluation point in the tested material. This problem is equivalent to determining the Fermat path between two given points in two bordering materials. It can be easily solved using a numerical algorithm looking for the minimum time of flight of ultrasonic waves between two given points.

The formula (13) gives the distribution of the ultrasonic field of a monochromatic wave with a circular frequency ω. To calculate the amplitude of short pulses generated by the real ultrasonic probes, we need to calculate $v(\boldsymbol{x}, \omega_k)$ for several discrete frequencies ω_k contained in the frequency spectrum of the transmitting transducer, then multiply them by the corresponding amplitudes of the spectrum, and finally perform the inverse Fast Fourier Transform. This way we can calculate the pulse shape in the time domain and finally obtain its maximum amplitude.

5. Calculation of pulse echo amplitude from model defects

Calculation of the ultrasonic field generated by the ultrasonic probe in the tested material is a very important aspect of the theoretical modeling of ultrasonic NDT inspection. It allows checking if potential defects are within the sensitivity zone of the selected probes and precisely adjusting its basic parameters (central frequency, transducer size, and refraction angle) to properly cover the inspection zone. However, illuminating the defect with a strong ultrasonic beam is not a sufficient condition for its detection in ultrasonic examination. The shape, orientation, and size of the defect are also of great importance. In the case of railway rails, most defects are relatively large cracks with varied size and orientation. To reasonably simulate such types of defects, we introduced model defects in the form of circles, squares, and rectangles of defined size and orientation. We also assume that the model defect surface is flat and stress-free. To calculate the amplitude of ultrasonic echo reflected from the model defect, we make

use of the reciprocity theorem presented by (Auld, 1979) and modified by (Schmerr, 2016), which is more suitable for NDT applications. The reciprocity theorem greatly reduces the complexity of the calculation of ultrasonic pulse echo amplitude in comparison to the direct approach requiring successive calculations of the ultrasonic field generated by the transmitting transducer incident on the defect, then assessment of the scattered field from the defect, and finally the integration of this field over the surface of the receiving transducer.

The general formula derived by (Schmerr, 2016) gives the voltage amplitude $V_R(\omega)$ generated on the receiving transducer by the ultrasonic wave reflected from the model defect. It is a definite integral over the surface of the model defect of the products of stress and particle velocity components of two elementary ultrasonic solutions:

$$V_R(\omega) = \frac{SF(\omega)}{\rho_1 V_{L1} S_T v_T^{(1)} v_R^{(2)}} \int_{S_d} \left(\tau_{ij}^{(1)} v_j^{(2)} - \tau_{ij}^{(2)} v_j^{(1)} \right) n_i \, dS \qquad (14)$$

where: $V_R(\omega)$ – voltage generated on the receiving transducer by ultrasonic waves reflected from the model defect, $v_j^{(1)}$ – components of particle velocity for solution (1), $v_j^{(2)}$ – components of particle velocity for solution (2), $\tau_{ij}^{(1)}$ – components of stress tensor for solution (1), $\tau_{ij}^{(2)}$ – components of stress tensor for solution (2), n_j – components of the unit vector **n** normal to the model defect, $v_T^{(1)}$ – amplitude of transmitting transducer vibrations for solution (1), $v_R^{(2)}$ – amplitude of receiving transducer vibrations for solution (2), S_T – surface area of the transmitting transducer, S_d – surface of the model defect, $SF(\omega)$ – system function, which incorporates the total effect of all electrical and electromechanical components of the ultrasonic system.

Solution (1) refers to the ultrasonic field generated in the tested material by the transmitting transducer, which physically interacts with the model defect and reflects at its surface. Actually,

it is the field we considered in the previous Chapter, which can be calculated using formula (13). Solution (2) refers to an imaginary (nonexistent) ultrasonic field that would be generated in the tested material if the receiving transducer acted as a transmitting transducer. The ultrasonic field calculated in the solution (2) neglects the presence of the defect and can be conveniently interpreted as the "sensitivity field" of the receiving transducer. In our dynamic model of ultrasonic testing, the solution (2) is generated by the same transducer but shifted on the x-axis by the ΔX value calculated using the formulas (3) and (8).

The general form of the reciprocity relation (14) cannot be directly used in practical modeling of ultrasonic inspection because it is dependent on some factors that are impossible or very difficult to determine based on information available to NDT personnel. This applies in particular to the system function $SF(\omega)$ and vibration amplitudes of transmitting and receiving transducer $v_T^{(1)}$ and $v_R^{(2)}$. We can simplify the formula (14) considering what is really necessary for modeling a real ultrasonic examination and what is unnecessary or excess information.

First of all, in NDT applications we don't need the absolute values of voltage generated on the receiving transducer $V_R(\omega)$ but only relations between voltage amplitudes received from modeled defects and from the defined reference reflector. This relation is commonly expressed on a logarithmic scale in decibels (dB). For this reason, in expression (14), we can ignore all constant values appearing before the integral sign. The system function $SF(\omega)$ cannot be neglected because this function carries important information about the bandwidth of the ultrasonic system. Principally, this function should be determined specifically for a given ultrasonic system (consisting of transmitter, receiver, probes, and cabling) using a special calibration procedure described by (Schmerr, 2016). Unfortunately, this procedure is rather difficult to perform, especially at the project design phase when the individual components of the modeled ultrasonic system may not be physically available. To overcome this difficulty, we

propose a simplified approach based only on information readily accessible from standard specifications of ultrasonic equipment.

Considering that probes used in ultrasonic testing of railway rails have frequencies within the limited range of 1 – 5 MHz we can safely assume that the typical ultrasonic receiver have in this range nearly flat frequency characteristic. The same can be said about the frequency band of a typical ultrasonic transmitter operating in a standard spike mode. Then we can safely assume that the shape of the system function $SF(\omega)$ is mainly determined by the frequency spectrum of the ultrasonic probe. According to (EN ISO 22232-2, 2021), the frequency spectrum of an ultrasonic probe is defined by the -6 dB frequency band measured in specified standard conditions. For commercial probes the parameter called relative frequency bandwidth BW is usually listed in the technical data sheets and easily accessible to NDT personnel.

Based on the probe bandwidth parameter BW and probe central frequency f_0 we can approximately determine the system function SF in the form of the Gaussian function:

$$SF(\omega) = e^{-\frac{(\omega/\omega_0)^2}{2\sigma^2}}, \qquad (15)$$

where $\omega_0 = 2\pi f_0$ and $\sigma = BW/235$. The shape of the Gaussian function reasonably resembles the typical shape of ultrasonic transducer frequency characteristics, and the σ parameter was chosen so that the half-width of this function is equal to the -6 dB bandwidth of the modeled transducer. Although the function (15) is only a rough approximation of the actual system function, it takes into account the most important factor determining the ultrasonic system frequency characteristic, that is the bandwidth of the ultrasonic probe.

Another simplification that can be applied to equation (14) follows from the fact that we are considering crack-like model defects. It means that the defect surfaces are stress-free, and in equation (14), we can put $\tau_{ij}^{(1)} \equiv 0$. After all the above simplifications, we can rewrite equation (14) in a much simpler form:

$$V_R(\omega) = -SF(\omega) \int_{S_d} \tau_{ij}^{(2)} v_j^{(1)} n_i \, dS, \tag{16}$$

where the system function $SF(\omega)$ is given by equation (15) and the minus sign is irrelevant because in our model all constants before the integral sign can be ignored.

Now the calculation of components of the stress tensor $\tau_{ij}^{(2)}$ on the surface of the model defect will be presented. These stress components are not zero because solution (2) in the reciprocity formula ignores the existence of defects in the tested material. So, we just need to calculate the ultrasonic field of the receiving transducer for the defect-free elastic solid and express it in the form of stress tensor components.

The general stress-strain relation for elastic solid is:

$$\tau_{ij}^{(2)} = C_{ijkl} e_{kl}^{(2)} = C_{ijkl} \frac{1}{2} \left(\frac{\partial u_k^{(2)}}{\partial x_l} + \frac{\partial u_l^{(2)}}{\partial k} \right) = C_{ijkl} \frac{\partial u_k^{(2)}}{\partial x_l}, \tag{17}$$

where: $u_k^{(2)}$ – components of displacement vector for solution (2), $e_{kl}^{(2)}$ – components of strain tensor for solution (2), C_{ijkl} – components of stiffness tensor for tested material.

For isotropic solid, components of the stiffness tensor can be expressed in much simpler form:

$$C_{ijkl} = \lambda \delta_{ij} \delta_{kl} + \mu \left(\delta_{ik} \delta_{jl} + \delta_{il} \delta_{jk} \right), \tag{18}$$

where: λ, μ – Lame elastic constants for the tested material, δ_{kl} – delta Kronecker symbol.

Substituting (18) to (17) we obtain:

$$\tau_{ij}^{(2)} = \lambda \delta_{ij} \frac{\partial u_k^{(2)}}{\partial x_k} + \mu \left(\frac{\partial u_i^{(2)}}{\partial x_j} + \frac{\partial u_j^{(2)}}{\partial x_i} \right). \tag{19}$$

In the next step, the expressions for partial derivatives of the components of the displacement vector appearing in (19), would be determined. At this step the initial assumption that the ultrasonic field generated by the probe at the model defect may be locally approximated by the plane wave can be implemented. In the considered case, it is the plane wave of transversal type with direction vector $e^{(2)}$, polarization vector $d^{(2)}$, and wave number k_2. The geometrical configuration for solutions (1) and (2) is shown in Fig. 3.

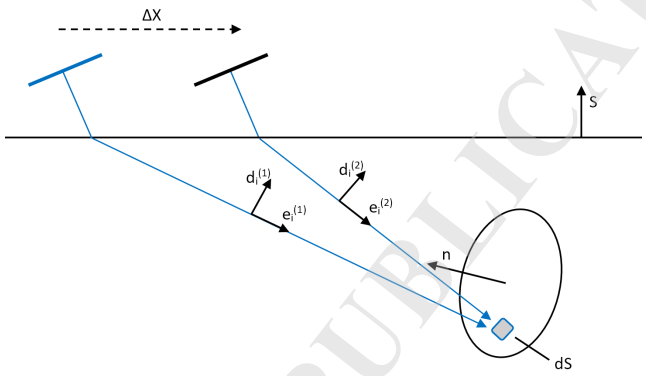

Fig. 3. Illustration supporting calculation of pulse-echo amplitude using reciprocity principle.

In this case, it can be put:

$$\boldsymbol{u}^{(2)} = \frac{1}{-i\omega}\boldsymbol{d}^{(2)}v^{(2)}(\boldsymbol{x},\omega), \qquad (20)$$

where: $u^{(2)}$ – displacement vector of local plane wave of solution (2), $d^{(2)}$ – polarization unit vector of local plane wave of solution (2), $v^{(2)}(\boldsymbol{x},\omega)$ – amplitude of local plane wave approximating solution (2).

Consequently, the partial derivatives of displacement field (20) can be expressed as:

$$\frac{\partial u_i^{(2)}}{\partial x_j} = \frac{ik_2}{-i\omega}d_i^{(2)}e_j^{(2)}v^{(2)}(\boldsymbol{x},\omega) = \frac{-1}{V_T}d_i^{(2)}e_j^{(2)}v^{(2)}(\boldsymbol{x},\omega), \qquad (21)$$

where: k_2 – wavenumber for transversal wave in tested material and V_T – velocity of transversal wave in tested material.

Substituting (21) into (19) we obtain:

$$\tau_{ij}^{(2)} = v^{(2)}(x,\omega)\frac{-1}{V_T}\left[\lambda\delta_{ij}d_i^{(2)}e_j^{(2)} + \mu\left(d_i^{(2)}e_j^{(2)} + d_j^{(2)}e_i^{(2)}\right)\right]. \quad (22)$$

The first component in square brackets is a scalar product of the polarization and directional vectors of the shear wave and must identically equal zero. Consequently, the final expression for stress components of solution (2) discussed in formulas (14), (16), (17), (19) takes the form:

$$\tau_{ij}^{(2)} = \frac{-\mu}{V_T}v^{(2)}(\boldsymbol{x},\omega)\left(d_i^{(2)}e_j^{(2)} + d_j^{(2)}e_i^{(2)}\right). \quad (23)$$

The scalar amplitude $v^{(2)}(\boldsymbol{x},\omega)$ of the particle velocity can be calculated from integral (13) by replacing the transmitting transducer with the receiving transducer shifted from the initial position (0,0,0) to the receiving position (ΔX,0,0), where ΔX must be calculated from the formula (10). The directional vector $\boldsymbol{e}^{(2)}$ can be calculated based on the positions of the center of the receiving transducer and a current integration point on the defect surface. The polarization vector $\boldsymbol{d}^{(2)}$ is perpendicular to the direction vector $\boldsymbol{e}^{(2)}$ and is lying in the vertical plane of incidence. It may be calculated from the formula:

$$\boldsymbol{d}^{(2)} = \frac{\boldsymbol{e}^{(2)}\times\mathbf{s}}{|\boldsymbol{e}^{(2)}\times\mathbf{s}|}\times\boldsymbol{e}^{(2)}, \quad (24)$$

where $\boldsymbol{s}$ is in the unit vector normal to the tested object surface (see Fig. 3). This way it is shown how to calculate the stress tensor components appearing in the reciprocity formula (14).

Now the particle velocity components $v_i^{(1)}$ appearing in formula (14) would be determined. These are the components of solution (1), which takes into account the interaction between the ultrasonic wave generated by the transmitting transducer and the embedded model defect. The exact solution to this type of problem is very difficult, even for simple model defects. To solve this problem in a simplified way, Kirchhoff approximation would be applied. In Kirchhoff approximation, the interaction of the ultrasonic beam with the material discontinuity is treated as the interaction of a (locally) plane wave with the plane boundary in the propagation medium. Such seminal problems have well-known solutions given by reflection and refraction coefficients (Auld, 1973 and Schmerr, 2016). In the model presented in this paper, crack-like planar defects with transverse dimensions considerably larger than the ultrasonic wavelength is considered. According to an in-depth analysis of the Kirchhoff approximation given by (Huang *et al.*, 2006), it should give reasonably accurate results in modeling such types of defects.

The calculation details of the vector $\nu^{(1)}$ can be found in (Katz *et al.*, 2021). Below, the highlighting the most important steps of derivation of the final formula, will be shown.

The wave approaching to certain small element dS on the defect surface can be characterized by its direction vector $\boldsymbol{e}_i^{(1)}$ unit polarization vector $\boldsymbol{d}_i^{(1)}$ and an amplitude of the particle velocity $v_i^{(1)}$. The coordinates of these vectors can be calculated from the positions of the center of the transmitting transducer and the center of the element dS on the defect surface. Then the incident wave is decomposed into two standard polarities considered in relation to the plane of the dS element, *SV* (shear vertical) and *SH* (shear horizontal), with polarization vectors of $\boldsymbol{d}_{iSV}$ and $\boldsymbol{d}_{iSH}$. It is important to note that $\boldsymbol{d}_{iSV}$ and $\boldsymbol{d}_{iSH}$ are not unit vectors but the mutually perpendicular vector components whose sum gives the unit directional vector of the incident wave:

$$\boldsymbol{d}_i^{(1)} = \boldsymbol{d}_{iSV}^{(1)} + \boldsymbol{d}_{iSH}^{(1)}. \tag{25}$$

First, let's consider the incident wave of *SV* type. For such a type of wave, there are generally two reflected waves, *SV* and *L* type. The *SV* wave reflects at an angle equal to the incidence angle, and its directional vector $\boldsymbol{e}_{rSV}$ and polarization vector $\boldsymbol{d}_{rSV}$ can be calculated from the knowledge of $\boldsymbol{e}_i$ and $\boldsymbol{d}_{iSV}$. The reflection coefficient for this type of wave, $R^{(SV,SV)}$, can be calculated from the standard formula for plane waves, as in (Schmerr, 2016), based on the incidence angle on the defect surface. The *L*-type wave reflects at an angle that can be calculated from Snell's law. The polarization direction of that wave is parallel to the propagation direction $\boldsymbol{e}_{rL}$. The reflection coefficient $R^{(L,SV)}$ can be calculated from the standard formula. These three waves are summed up to give the first part of the solution (1) arising from the *SV* component of the incident wave:

$$\boldsymbol{v}_{SV}^{(1)} = v^{(1)}\big(\boldsymbol{d}_{iSV} + R^{(SV,SV)}\,\boldsymbol{d}_{rSV} + R^{(P,SV)}\,\boldsymbol{d}_{rL}\big). \tag{26}$$

The vectors $\boldsymbol{d}_{rSV}$ and $\boldsymbol{d}_{rL}$ are not of the unit length but have the same reduced length as the vector $\boldsymbol{d}_{iSV}$. Then, let's consider the incident wave of *SH* type. For such incident wave there is only one reflected wave of *SH* type. The *SH* wave reflects at an angle equal to the incidence angle and its polarization vectors are given by:

$$\boldsymbol{d}_{rSH} = \boldsymbol{d}_{iSH}. \tag{27}$$

The vector $\boldsymbol{d}_{rSH}$ is not of a unit length but has a reduced length, the same as the vector $\boldsymbol{d}_{iSH}$. Based on the above, an expression for the second part of the solution (1) caused by the *SH* polarization of the incident wave can be written:

$$\boldsymbol{v}_{SH}^{(1)} = v^{(1)}\big(\,\boldsymbol{d}_{iSH} + R^{(SH,SH)}\,\boldsymbol{d}_{rSH}\big). \tag{28}$$

Having calculated particle velocities for both polarizations of the incident wave, the total particle velocity of the ultrasonic vibration for the solution (1) can be written as:

$$\boldsymbol{v}^{(1)} = \boldsymbol{v}_{SV}^{(1)} + \boldsymbol{v}_{SH}^{(1)} = v^{(1)}\big(\boldsymbol{d}^{(1)} + R^{(SV,SV)}\,\boldsymbol{d}_{rSV} + R^{(SH,SH)}\,\boldsymbol{d}_{rSH} + R^{(P,SV)}\,\boldsymbol{d}_{rL}\big) \tag{29}$$

To simplify the notation, all the vectors defining the polarizations and relative amplitudes of waves acting on the defect surface can be grouped into one vector $\boldsymbol{D}^{(1)}$:

$$\boldsymbol{D}^{(1)} = \boldsymbol{d}^{(1)} + R^{(SV,SV)}\,\boldsymbol{d}_{rSV} + R^{(SH,SH)}\,\boldsymbol{d}_{rSH} + R^{(P,SV)}\,\boldsymbol{d}_{rL} \tag{30}$$

Similarly, the expression for $v^{(1)}$ can be rewritten as:

$$\boldsymbol{v}^{(1)} = v^{(1)}(x,\omega)\boldsymbol{D}^{(1)} \tag{31}$$

At this stage we have determined all the elements necessary for the reciprocity formula (14), which may be rewritten in a more straightforward form where we also neglected all constants before the integral sign:

$$V_R(\omega) = SF(\omega)\int_{S_d} v^{(1)}v^{(2)}\big[\big(\boldsymbol{D}^{(1)}\cdot\boldsymbol{d}^{(2)}\big)\big(\boldsymbol{e}^{(2)}\cdot\boldsymbol{n}\big) + \big(\boldsymbol{D}^{(1)}\cdot\boldsymbol{e}^{(2)}\big)\big(\boldsymbol{d}^{(2)}\cdot\boldsymbol{n}\big)\big]\,dS, \tag{32}$$

where: $v^{(1)}(x,\omega)$ – amplitude of solution (1) calculated from the formula (11) for transmitting

transducer in position (0,0,0), $v^{(2)}(x,\omega)$ – amplitude of solution (2) calculated from the formula (11) for receiving transducer in position (ΔX,0,0), $\mathbf{D}^{(1)}$ – polarization vector for the solution (1), $\mathbf{d}^{(2)}$ – polarization vector for the solution (2).

Integral (32) provides a workable solution for numerical calculations of amplitudes of ultrasonic echoes reflected from the planar model defects of any size and orientation. The main difference of this solution in relation to the known solutions obtained within the quasi-static ultrasonic model is that all the quantities related to solution (2) are calculated for the receiving position of the transducer, which is shifted by ΔX from the initial position where the ultrasonic transmission takes place. The formula (32) allows for the computation of receiving voltage at a fixed frequency ω. To calculate the signal waveform in the time domain, it is necessary to calculate $V_R(\omega_k)$ for the series of frequencies contained in the system function spectrum and then calculate the inverse Fourier transform using the FFT algorithm. Then, the maximum echo amplitude in the time domain can be determined.

6. Calculation of ultrasonic field generated by angle beam probes

The presented model allows for computer simulation of several important aspects of ultrasonic inspection of railway rails. The first basic functionality of the software is the calculation of ultrasonic fields generated in the tested material by ultrasonic probes with different parameters (frequency, refraction angle, transducer size, bandwidth, etc.). To illustrate this functionality, we calculated the ultrasonic fields of three angle beam probes that could be used for detecting transversal defects in the rail head. There were angle beam shear wave probes: T60°, T70°, and T80° of the same central frequency (f_0 = 2 MHz), bandwidth (BW = 50%), and transducer size (14x14 mm). The refraction wedges of all probes were made of PMMA. The probes can be

positioned on the rail head center, and their beams are directed along the plane of symmetry of the rail (*X*-*Y* plane).

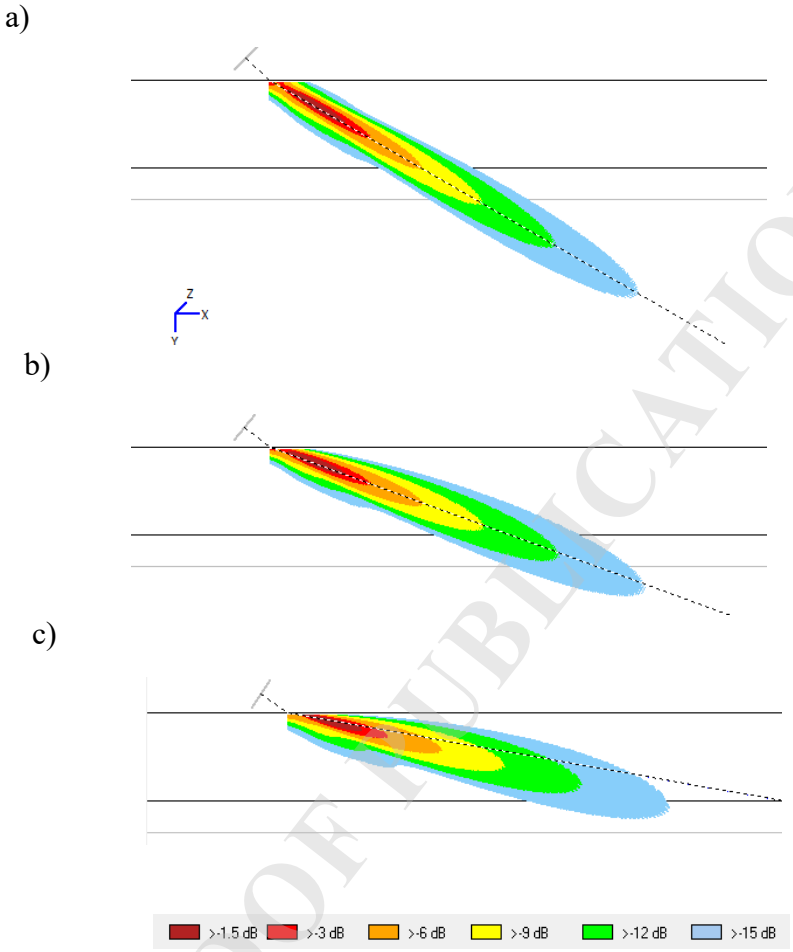

Fig. 4. Ultrasonic beam cross-sections for three similar angle beam probes with different refraction angles. a) 2T60-A14x14, b) 2T70-A14x14, c) 2T80-A14x14. The probe codes are explained in the text.

In Fig. 4, the beam cross-sections in the *X*-*Y* plane are illustrated with the color-coded maps of the particle velocity amplitude. It should be emphasized that there are distributions of maximum amplitudes of short pulses generated by the typical ultrasonic probes, not the amplitudes of a monochromatic wave of a single frequency. All field distributions are normalized to the maximum value in the field of a given probe, so the maps do not illustrate correctly the

differences in absolute amplitudes between different probes. Actually, the highest field amplitude is observed for the near-field maximum of the T60° probe. For the T70° probe, the maximum is only slightly smaller (0.2 dB), but for the T80° probe, it is reduced by 2.3 dB in comparison to the T60° probe.

Another interesting observation is the considerable deviation of the acoustic axis from the geometric axis (the dashed line on the field graphs) for the T80° probe. This is a manifestation of the fact that the transmission coefficient of ultrasonic waves on the wedge-material border quickly drops near the 2nd critical angle. Based on presented distributions of ultrasonic fields, one can draw the conclusion that using angle beam probes with nominal refraction angles higher than 70° - 75° would not be effective for detecting rail head transversal defects despite the fact that their nominal refraction angle is better suited to detecting vertical defects.

Figure 5 illustrates the ultrasonic beam cross sections for three T70° probes, distinguished solely by their frequency bandwidths *BW*: a narrow band probe (*BW* = 20%), a medium band probe (*BW* = 50%), and a broad band probe (*BW* = 90%).

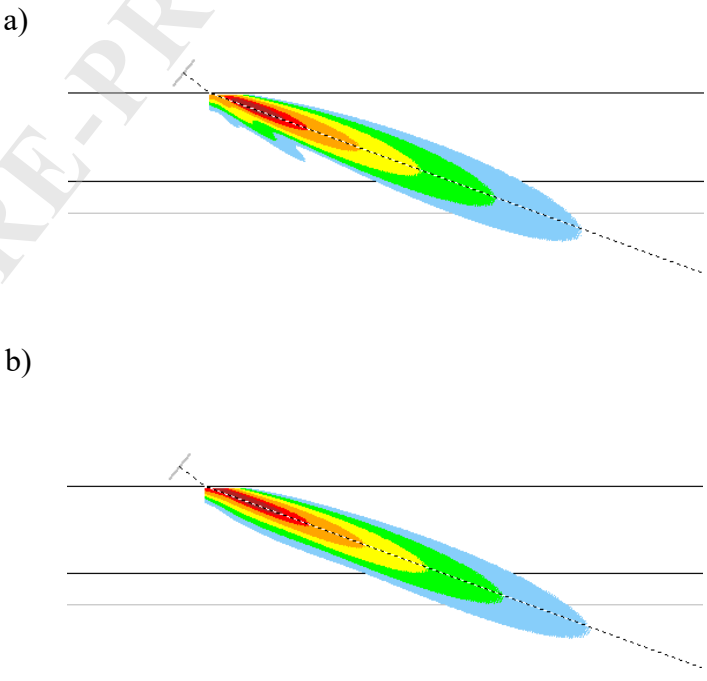

c)

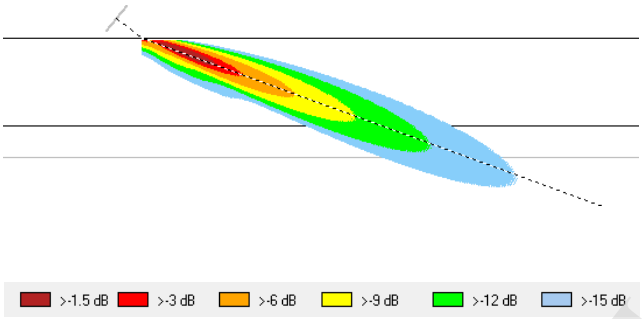

Fig. 5. Ultrasonic beam cross-sections for three 2T70-A14x14 type probe differing only in frequency bandwidths *BW*: a) *BW* = 20%, b) *BW* = 50%, c) *BW* = 90%.

Overall, the ultrasonic fields for all three probes are similar, with only one noticeable difference. The field for the narrow band probe, as shown in picture a), displays one side lobe below the main lobe. The ultrasonic fields of the other two probes are more uniform and do not exhibit any side lobes. The last example of using the simulation program for calculation of ultrasonic beams of angle beam probes concerns the influence of the attenuation coefficient of the rail material on the distribution of ultrasonic field. As mentioned in Paragraph 3 the attenuation coefficient of ultrasonic waves in rail steel was taken from the tables given in (Ono, 2020a) and (Ono, 2020b). These attenuation coefficient values are used as standard in our simulation program for calculation of ultrasonic field distributions. We have checked whether assuming a zero attenuation coefficient in railway steel would significantly affect the calculated ultrasonic fields.

On the Fig. 6 there are presented the ultrasonic beams of 2T70-A14x14 probe (*BW=50%*) calculated with attenuation coefficient taken from (Ono, 2020b) and attenuation coefficient assumed to be zero.

a)

b)

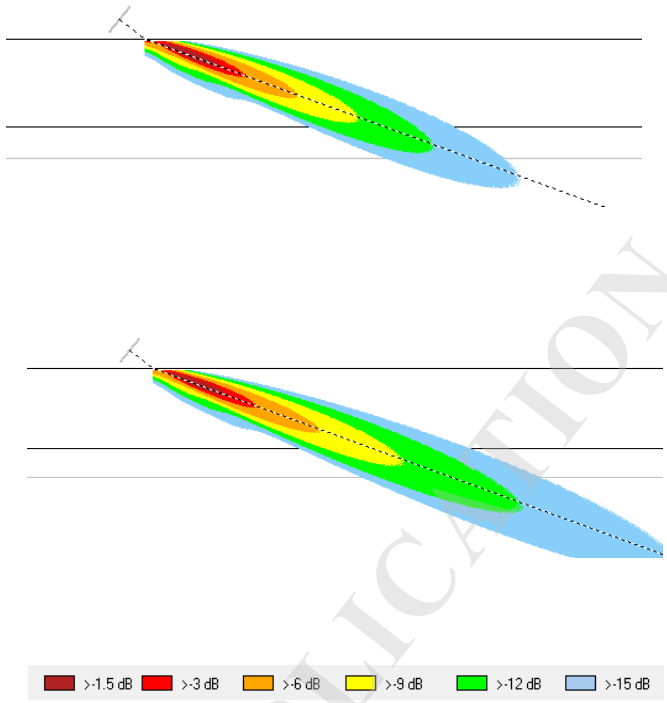

Fig. 6. Ultrasonic beam cross-sections for 2T70-A14x14 probe calculated with assumption of attenuation coefficient: a) taken from (Ono, 2020b) b) equal to zero.

As can be seen, attenuation coefficient have a considerable effect on distribution of ultrasonic field of typical 2 MHz shear waves probe commonly used in rail inspections. It means that the unjustified assumption of a zero attenuation coefficient of railway steel would lead to significant overestimation of the simulated field and misleading conclusions concerning the probe sensitivity zone.

7. Simulation of ultrasonic echo envelopes during rail scanning

The second fundamental feature of the discussed software is the calculation of ultrasonic echo amplitudes from simple model defects (circles, rectangles) of various sizes, orientations, and positions. Considering the operating principles of automated rail testing systems, the most

significant outcome of ultrasonic inspections is the echo envelope recorded for each testing probe while it moves along the rail over defect locations. Based on the amplitudes and shapes of the recorded envelopes, the defects are classified and displayed on the B-scan diagrams with the appropriate colors.

The software allows for the calculation of echo envelopes for defined ultrasonic probes moving along the rail axis over the simulated model defects. It calculates the echo amplitudes for the successive positions of the probe along the X axis in the points, which are determined by the scanning speed and repetition frequency of the testing system. In this way, the computer simulation closely imitates the operation of a real rail inspection system, taking into account its operating parameters.

We simulated echo envelopes for two different defects, one located in the rail head and the other in the rail foot. The main goal of the performed simulations was to show the differences between our new dynamic ultrasonic testing model and the standard quasi-static model. As the first example, we calculated the echo envelopes for the circular defect situated in the central part of the rail head which is supposed to simulate a common transversal defect of the rail head called tache ovale (Kumar, 2006). The center of the model defect was assumed at Y_d =15mm and its diameter D_d was 10 mm. It was assumed that the defect plane is deflected from the rail transversal plane by 10° towards the bottom of the rail (see Fig. 7).

The model defect was detected with the 2T70-A14x14 ultrasonic probe described in the previous Chapter. The probe was guided along the center of the rail head with its beam directed along the rail, parallel to the scanning direction. The simulated test configuration is illustrated in Fig. 7.

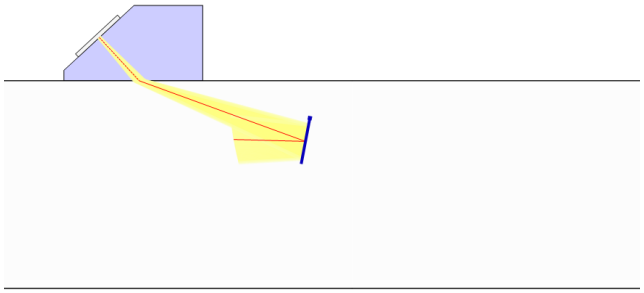

Fig. 7. The simulated probe - rail - defect configuration with circular defect of diameter D_d=10 mm deviated by θ=10° from the rail transversal plane.

As can be readily seen from Fig. 7, in the simple geometric approximation of ray tracing, the implemented defect would not be detected due to unfavorable orientation with respect to the incident beam. However, in the model presented in the following paper, which takes into account the diffraction phenomena, such defects can be detected with a reasonable echo amplitude.

In Fig. 8, the simulated pulse echo envelope calculated for the above testing configuration can be seen. The following assumptions were taken: the scanning speed: 80 km/h and the repetition frequency of the ultrasonic system:5 kHz. The black horizontal line on the chart shows the reference level representing the maximum amplitude of the pulse echo from the standard SDH (Side-Drilled Hole) reflector of 6 mm diameter situated 20 mm below the rail surface. The echo amplitude from such a cylindrical reflector was calculated using the model of (Lopez-Sanchez *et al*., 2025), because the model discussed in this paper was developed only for flat reflectors. This mixed approach implies that the test sensitivity of the ultrasonic system should be set up when the inspection wagon is stationary or is moving over the reference rail with a low speed. The triangles in Fig. 8 represent the points of the dynamic echo envelope, which would be registered by the ultrasonic system when scanning the rail at a speed of 80 km/h and a repetition rate of 5 kHz. The scanning direction is assumed to be parallel to the viewing direction of the

ultrasonic probe. For comparison, a continuous line shows the echo envelope calculated using the quasi-static ultrasonic model, which neglects the movement of the ultrasonic probe during the transmission-reception cycle.

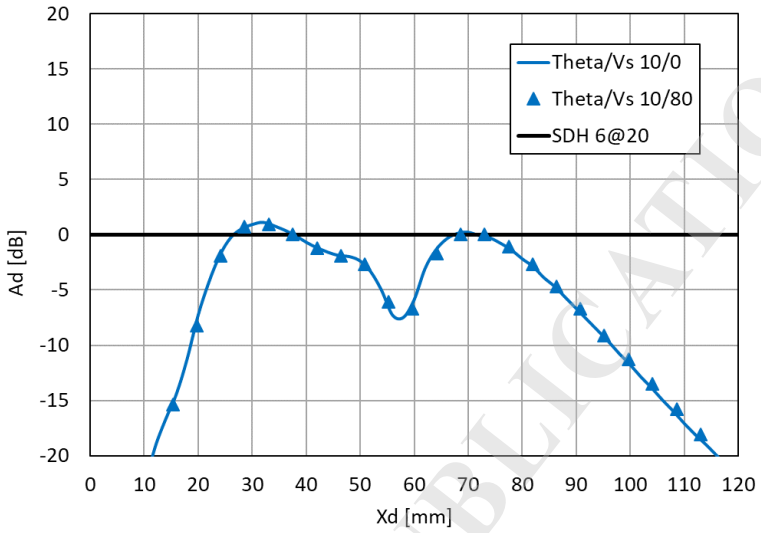

Fig. 8. The simulated echo envelope of the model defect (D=10 mm, θ=10°) detected with 2T70-A14x14 probe scanning the rail with speed of 80 km/h.

As can be seen, the main difference between the dynamic and the quasi-static model is the discretization of the echo envelope due to the fact that a 5 kHz system running with a speed of 80 km/h fires ultrasonic pulses every 4.4 mm along the rail length. The difference in amplitude for the corresponding points of both envelopes does not exceed 0.3 dB. It seems that a scanning speed of 80 km/h does not create major problems for the analyzed testing configuration. Therefore, in the next simulation, the scanning speed was increased to 160 km/h. The run of obtained echo envelopes is shown in Fig. 9. In this case, echo envelopes were calculated for both scanning directions, i.e., parallel and antiparallel to the viewing direction of the ultrasonic probe. In Fig 9. the black horizontal line on the chart showing the reference level representing the amplitude of the pulse echo from the standard SDH (Side

Drilled Hole) reflector is also presented. With higher testing speed, the problem of sparse sampling (in this case, every 8.9 mm) becomes more evident. It consists of the fact that a high echo amplitude from a given defect is recorded only at a few points, which may lead to uncertainty in the interpretation of the indications. This is because algorithms of automatic defect detection during rail scanning require several (often 5-6) consecutive echo registration cycles of signal level situated above the recording level to qualify the indication as significant. It means that the algorithms of indication discrimination should be carefully adjusted to the scanning speed based on the results of similar simulations.

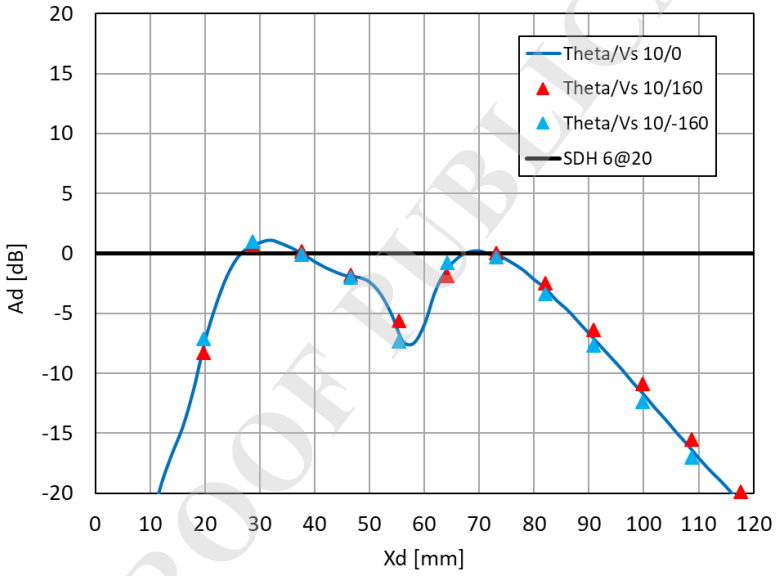

Fig. 9. The simulated echo envelopes of the model defect (D=10 mm, θ = 10°) obtained with T70-14x14 probe scanning the rail with speed of 160 km/h in two directions, i.e., parallel (red triangles) and antiparallel (blue triangles), to the viewing direction of the ultrasonic probe.

Another conclusion from the graphs presented in Fig. 9 is that the difference between the amplitudes of the envelopes calculated from the dynamic and quasi-static models increased to ± 0.7 dB. This difference is solely due to the fact that the ultrasonic probe moves during the transmitting-receiving cycle, and its sign depends on whether the movement is parallel or antiparallel to the viewing direction of the probe.

8. Conclusions

In the paper, the new theoretical model of ultrasonic testing with high scanning speed was presented. Unlike the standard quasi-static models used so far, it does not assume that the scanning speed of the ultrasonic probe is negligible in comparison to the speed of ultrasonic waves in the tested material. In consequence, it takes into account that the ultrasonic probe changes its position during the transmitting-receiving cycle of the ultrasonic system. The new model is based on well-established principles of ultrasonic theory, such as the Rayleigh-Sommerfeld integral, reciprocity relation, and the Kirchhoff approximation, but implements a new concept of variable probe position at the moments of pulse transmission and reception. The ΔX shift in the probe position is calculated based on the defect position relative to the probe at the pulse firing time, the probe scanning speed, and the speed of sound in the tested material.

The model allows for the calculation of the ultrasonic field generated by the probe in the tested material and the amplitudes of the ultrasonic echoes reflected from the simple model defects implemented in the tested material. Based on the theoretical model, the computer program *SymUT* was developed and designed specifically for the simulation of high-speed ultrasonic testing of railway rails in track. Thanks to the semi-analytical nature of the developed model, the program can be executed on standard PC computers with reasonably short computational times. It enables effective computer simulation of many test configurations and optimization of ultrasonic probes for detection of different types of defects occurring in railway rails.

In the last part of the paper, example simulations were presented and discussed in the context of increased speed of automated testing of rails. The simulations performed showed that the defect echo envelopes calculated from the quasi-static and dynamic models differ in two ways. Firstly, the echo envelopes calculated within the dynamic model are discrete, which is a direct

consequence of the limited repetition frequency (c.a. 5 kHz) of the ultrasonic system. The sparse sampling along the rail length can reduce the detectability of some defects and requires modification of automated indication discrimination algorithms. On the other hand, the differences in echo amplitudes in corresponding points of envelopes calculated according to dynamic and quasi-static models are not too big and reach 3 dB for a scanning speed of 160 km/h. In general, it can be stated that there are no fundamental physical obstacles to increasing the speed of automatic testing of railway rails to 160 km/h, assuming that the technical problems related to the mechanical guidance of the probes and their acoustic coupling are solved.

Acknowledgments

The paper was written as a result of the implementation of the Project no. BRIK2/0013/2022, "A joint undertaking of the National Centre for Research and Development - PKP Polskie Linie Kolejowe S.A. to support scientific research and development work in the area of railway infrastructure, entitled Research and Development in Railway Infrastructure BRIK II".

References

1. Auld B.A. (1973), *Acoustic Fields and Waves in Solids*, p. 167, John Wiley & Sons, ISBN 5885013438.

2. Auld B.A. (1979), General electromechanical reciprocity relations applied to the calculation of elastic waves scattering coefficients. *Wave Motion,* **1**(1): 3–10, https://doi.org/10.1016/0165-2125(79)90020-9(access: 28.10.2025).

3. Calmon P., Lhemery A., Lecoeur-Taibi I., Raillon R., Paradis L. (1998), Models for the computation of ultrasonic fields and their interaction with defects in realistic NDT configurations, *Nuclear Engineering and Design* **180**(3): 271–283, https://doi.org/10.1016/S0029-5493(97)00299-9 (access: 28.10.2025).

4. Darmon M., Chatillon S. (2013), Main Features of a Complete Ultrasonic Measurement Model: Formal Aspects of Modeling of Both Transducers Radiation and Ultrasonic Flaws

Responses. *Open Journal of Acoustics* **3**(3A): 43-53, https://doi.org/10.4236/oja.2013.33A008 (access: 28.10.2025).

5. Deschamps G.A. (1972), Ray techniques in electromagnetics. *Proceedings of the IEEE* **60**(9): 1022–1035, https://doi.org/10.1109/PROC.1972.8850 (access: 28.10.2025).

6. EN 16729-1 (2016) *Railway applications – Infrastructure – Non-destructive testing on rails in track* – Part 1: Requirements for ultrasonic inspection and evaluation principles, CEN, Brussels. https://www.en-standard.eu/une-en-16729-1-2016-railway-applications-infrastructure-non-destructive-testing-on-rails-in-track-part-1-requirements-for-ultrasonic-inspection-and-evaluation-principles/(access: 28.10.2025).

7. EN 16729-3 (2018), *Railway applications – Infrastructure – Non-destructive testing on rails in track – Part 3: Requirements for identifying internal and surface rail defects,* CEN, Brussels, https://www.en-standard.eu/csn-en-16729-3-railway-applications-infrastructure-non-destructive-testing-on-rails-in-track-part-3-requirements-for-identifying-internal-and-surface-rail-defects/ (access: 28.10.2025).

8. EN ISO 22232-2 (2021) *Non-destructive testing - Characterization and verification of ultrasonic test equipment - Part 2: Probes*, ISO, https://www.iso.org/obp/ui/es/#iso:std:iso:22232:-2:ed-1:v1:en (access: 28.07.2023).

9. Gengembre N., Lhemery A, (2000), Pencil method in elastodynamics: application to ultrasonic field computation, *Ultrasonics* **38**, (1-8): 485-499, Eslevier page: PII S0041-624X(99)00068-2
(access: 28.10.2025).

10. Heckel T., Casperson R., Rühe S., Mook G. (2018), Signal Processing for Non-Destructive Testing of Railway Tracks, [in:] *Proceedings of 44th Annual Review of Progress in Quantitative Nondestructive Evaluation,* **37**, 1949, https://doi.org/10.1063/1.5031528 (access: 28.10.2025).

11. Huang R., Schmerr L.W., Sedov A., Gray T.A. (2006), Kirchoff Approximation Revisited – Some New Results For Scattering in Isotropic and Anisotropic Elastic Solids. *Research in*

Nondestructive Evaluation **17**(3): 137–160, https://doi.org/10.1080/09349840600787956 (access: 28.10.2025).

12. Katz T., Mackiewicz S., Ranachowski Z., Kowalewski Z.L., Antolik Ł. (2021) Ultrasonic detection of transversal cracks in rail heads - theoretical approach. Engineering Transactions **69**(4): 437-456. https://doi.org/10.24423/EngTrans.1695.20211220 (access: 28.10.2025).

13. Kumar S., (2006), Study of rail breaks: Associated risks and maintenance strategies. *Technical report*. Division of Operation and Maintenance Engineering Lulea Railway Research Center (JVCT) Lulea University of Technology, Sweden. ISSN: 1402-1536, https://www.diva-portal.org/smash/get/diva2:995250/FULLTEXT01.pdf (access: 28.10.2025).

14. Lopez-Sanchez A.L., Kim H.J., Schmerr L.W., Sedov A. (2005) Measurement Models and Scattering Models for Predicting the Ultrasonic Pulse-Echo Response From Side-Drilled Holes. *Journal of Nondestructive Evaluation* **24**(3): 83-96, https://doi.org/10.1007/s10921-005-7658-4 (access: 28.10.2025).

15. Mackiewicz S., Ranachowski Z., Katz T., Dębowski T., Starzyński G., Ranachowski P., (2024) Modeling of Acoustic Coupling of Ultrasonic Probes for High-Speed Rail Track Inspection. Archives of Acoustics **49**(2): 255-266, https://doi.org/10.24425/aoa.2024.148787.

16. Ono K. (2020a), A Comprehensive Report on Ultrasonic Attenuation of Engineering Materials, Including Metals, Ceramics, Polymers, Fiber-Reinforced Composites, Wood and Rocks. *Applied Sciences,* **10**(7), 2230. https://dx.doi.org/10.3390/app10072230 (access: 28.10.2025).

17. Ono K. (2020b) Dynamic Viscosity and Transverse Ultrasonic Attenuation of Engineering Materials, *Applied Sciences* **10**(15), 5265. https://dx.doi.org/10.3390/app10155265 (access: 28.10.2025).

18. Raillon R., Lecoeur-Taibi I. (2000), Transient elastodynamic model for beam defect interaction: application to nondestructive testing. *Ultrasonics,* **38**(1–8): 527–530, https://doi.org/10.1016/S0041-624X(99)00067-0 (access: 28.10.2025).

19. Schmerr Jr. L. W. (2016), *Fundamentals of Ultrasonic Nondestructive Evaluation. A modelling approach,* 2nd ed., Springer Nature, Basel. https://doi.org/10.1007/978-3-319-30463-2 (access: 28.10.2025).

20. Thomas H.M., Heckel T., Hanspach G. (2007), Advantage of a combined ultrasonic and eddy current examination for railway inspection trains. *Insight,* **49**(6): 341-344. http://dx.doi.org/10.1784/insi.2007.49.6.341 (access: 28.10.2025).

21. UIC Code 712-R (2002) *Rail Defects*, 4th ed. UIC, https://www.scribd.com/document/338561091/UIC-Code-712-R-2002-Rail-Defects (access: 28.10.2025)

22. Zumpano G, Meo M (2006) A new damage detection technique based on wave propagation for rails. International Journal of Solids and Structures 43(5):1023–1046. https://doi.org/10.1016/j.ijsolstr.2005.05.006.